Mg^{2+}-Induced tRNA Folding[†,‡]

Victor Serebrov,[§] Ronald J. Clarke,[||] Hans J. Gross,[⊥] and Lev Kisselev*[,§]

Engelhardt Institute of Molecular Biology, Moscow 119991, Russia, Max Planck Institute für Biophysik, D-60596 Frankfurt am Main, Germany, and Institut für Biochemie, Bayerische Julius Maximilians Universität, Biozentrum, Am Hubland, D-97074 Wurzburg, Germany

Received September 25, 2000; Revised Manuscript Received March 2, 2001

ABSTRACT: Mg^{2+}-induced folding of yeast $tRNA^{Phe}$ was examined at low ionic strength in steady-state and kinetic experiments. By using fluorescent labels attached to tRNA, four conformational transitions were revealed when the Mg^{2+} concentration was gradually increased. The last two transitions were not accompanied by changes in the number of base pairs. The observed transitions were attributed to Mg^{2+} binding to four distinct types of sites. The first two types are strong sites with K_{diss} of 4 and 16 μM. The sites of the third and fourth types are weak with a K_{diss} of 2 and 20 mM. Accordingly, the Mg^{2+}-binding sites previously classified as "strong" and "weak" can be further subdivided into two subtypes each. Fluorescent transition I is likely to correspond to Mg^{2+} binding to a unique strong site selective for Mg^{2+}; binding to this site causes only minor A_{260} change. The transition at 2 mM Mg^{2+} is accompanied by substantial conformational changes revealed by probing with ribonucleases T1 and V1 and likely enhances stacking of the tRNA bases. Fast and slow kinetic phases of tRNA refolding were observed. Time-resolved monitoring of Mg^{2+} binding to tRNA suggested that the slow kinetic phase was caused by a misfolded tRNA structure formed in the absence of Mg^{2+}. Our results suggest that, similarly to large RNAs, Mg^{2+}-induced tRNA folding exhibits parallel folding pathways and the existence of kinetically trapped intermediates stabilized by Mg^{2+}. A multistep scheme for Mg^{2+}-induced tRNA folding is discussed.

An intriguing feature of biopolymers is their ability to acquire three-dimensional structures of unique and irregular shapes that are efficient in molecular recognition and catalysis. Although the majority of studies are focused on protein folding, RNA folding is also of great interest due to the key role of RNAs in many cellular structures and processes. In contrast to most proteins, RNAs can adopt their folded state only if complexed with mono- and bivalent cations and/or polycations, like polyamines, required to overcome the electrostatic repulsion of negatively charged RNA chains. While binding of monovalent cations to RNA is predominantly unspecific, that of bivalent cations and polyamines is site-specific (*1*, *2*). Spermine molecules and Mg^{2+} ions are coordinated in specific negatively charged binding pockets as seen in the X-ray structure of yeast $tRNA^{Phe}$ (*3*, *4*).

Mg^{2+} ions play a key role in RNA folding and often provide catalytically reactive centers or the correct conformation of functionally important elements of RNA structure. Most classes of catalytic RNAs, such as hammerhead ribozymes and group I introns, require Mg^{2+} for both folding and catalysis and therefore can be regarded as metalloenzymes (*5*, *6*). The discovery of ribozymes, in which the catalytic activity results from unique folding of the RNA chain and from coordination of Mg^{2+} at specific sites, inspires growing interest in Mg^{2+}-induced RNA folding. It was demonstrated that Mg^{2+}-induced folding of large RNAs involves a number of kinetically distinct steps (*7*−*9*). Parallel folding pathways may exist and cause formation of misfolded species (*10*, *11*).

For several decades tRNA was the most extensively studied RNA molecule. X-ray data on individual tRNAs provide a detailed view of the tRNA molecule that most likely represents its actual native state in solution. Numerous studies of Mg^{2+} binding to tRNA in solution revealed the role of Mg^{2+} in stabilization of tRNA structural elements. For many tRNAs, the discrete steps of tRNA heat-induced unfolding have been assigned to melting of distinct structural elements, and the effect of Mg^{2+} on their stability has been revealed in steady-state and kinetic studies (reviewed in ref *12*). The general scheme of tRNA folding proposed in these studies suggests that in the absence of Mg^{2+} and at a moderate ionic strength an equilibrium occurs between two conformations. One of these conformations possesses the complete set of base pairs and intact structural elements. In the other conformation the tertiary structure and the D-stem are melted (the "semidenatured state"). The equilibrium between these two conformations represents the early melting transition of tRNAs, which occurs at nearly physiological temperatures for most tRNAs and is usually well separated from melting of the cloverleaf secondary structure (*13*, *14*). The semidenatured conformation lacking the tertiary structure and D-stem base pairing but still containing most of the

[†] Supported by the Volkswagen Foundation. V.S. was awarded a Robert Havemann Scholarship. R.J.C. was supported by the Max Planck Society.

[‡] Dedicated to the memory of Professor Oleg B. Ptitsyn.

* To whom correspondence should be addressed. E-mail: kissel@imb.imb.ac.ru. Fax: (7 095) 135 1405. Tel: (7 095) 135 6009.

[§] Engelhardt Institute of Molecular Biology.

[||] Max Planck Institute für Biophysik. Present address: School of Chemistry, University of Sydney, NSW 2006, Australia.

[⊥] Bayerische Julius Maximilians Universität.

10.1021/bi002241p CCC: $20.00
Published on Web 05/10/2001

secondary structure elements resembles the molten globule state known for globular proteins (*15*, *16*). The tight binding of Mg^{2+} to the native state strongly stabilizes the tertiary structure so that its melting temperature surpasses that of the remaining secondary structure, and then the whole structure melts in the two-state manner. Solution studies of tRNA stabilization by Mg^{2+} demonstrated that at moderate temperatures the presence of 10^{-4} M Mg^{2+} is sufficient to completely shift the equilibrium toward the native tRNA state with all strong Mg^{2+}-binding sites occupied (*17*−*19*).

According to the outlined general scheme, submillimolar concentrations of Mg^{2+} are sufficient to maintain the native tRNA structure. However, to gain the maximal efficiency, almost all in vitro processes involving tRNA require the presence of millimolar Mg^{2+}. Therefore, it is suggested that weak Mg^{2+} binding occurring at millimolar Mg^{2+} concentrations notably contributes to tRNA folding and is important for accomplishment of the conversion into the native state. Here, we focus on the Mg^{2+}-induced tRNA folding in terms of distinct steps of native structure formation as a result of Mg^{2+} binding to strong and weak sites and search for possible intermediates in this process. It is also tempting to reveal possible differences between recently studied folding of large RNAs and fairly short RNAs, like tRNAs.

MATERIALS AND METHODS

Yeast $tRNA^{Phe}$ was isolated from total yeast tRNA (Boehringer Mannheim) using BD-cellulose chromatography (*20*). Further purification was achieved either by preparative denaturing polyacrylamide gel electrophoresis or by two sequential chromatographic steps on a DEAE 3SW HPLC column (Pharmacia) in the presence of 7 M urea and EDTA. In all further experiments doubly distilled water passed through a Millipore water purification system was used for RNA storage, buffer solutions, etc. To remove traces of bivalent metals, tRNA was heated at 60 °C in the presence of 1 mM EDTA for 1 min and then precipitated with ethanol.

Fluorescent Labeling of $tRNA^{Phe}$. This procedure was performed in three steps: (1) generation of an amino reactive site at the labeling position by appropriate chemical treatment, (2) incorporation of carbohydrazide, and (3) coupling of fluorescein isothiocyanate (FITC)[1] with the generated amino group. Carbohydrazide, sodium borohydride, sodium periodate, and FITC were purchased from Sigma.

Position 76. The terminal ribose of $tRNA^{Phe}$ was oxidized with sodium periodate (*21*) followed by reaction with carbohydrazide and FITC as described (*22*).

Position 37. Wybutine was excised by incubation of $tRNA^{Phe}$ at pH 2.8 for 3 h (*23*) followed by incubation with carbohydrazide (2 mg/mL) in 0.2 M sodium acetate, pH 5.6, for 1 h at 37 °C. After ethanol precipitation tRNA was dissolved in 40 mM HEPES−KOH, pH 8.0, and 30% DMSO. FITC was added to a final concentration of 1 mg/mL, and the reaction was run for 2 h at 37 °C.

Positions 16 and 17. Dihydrouracils were reduced with sodium borohydride (*23*). Reaction with carbohydrazide and FITC was performed as described above for wybutine, but reaction with carbohydrazide was conducted in the presence of 0.2 M sodium acetate, pH 4.3. After reaction with FITC and 2-fold precipitation with ethanol, tRNA was subjected to preparative gel electrophoresis, and the fluorescent band was cut out and eluted. To remove traces of acrylamide, the solution was extracted with water-saturated phenol and tRNA was ethanol-precipitated.

Steady-State and Slow Kinetic Measurements. All measurements if not indicated otherwise were carried out in HEPES−KOH, pH 7.8 at 20 °C. For fluorescent measurements, a Shimadzu RF-5301 spectrofluorimeter with a thermostated cell holder was used. Fluorescein fluorescence was measured at 515 nm; the excitation was at 485 nm. Mg^{2+} binding to tRNA was monitored using the fluorescent indicator 8-hydroxyquinoline-5-sulfonic acid (HQS). Calculation of the number of bound Mg^{2+} per tRNA molecule was performed as described (*18*). The indicator fluorescence was registered at 500 nm with excitation at 350 nm.

Absorbance of tRNA was measured using a Shimadzu 1601 spectrophotometer. For slow kinetic measurements, small volumes of a Mg^{2+} stock solution were added to the cell containing tRNA, and the solution was mixed vigorously. The dead time did not exceed 5 s in most experiments.

Stopped-Flow Experiments. Stopped-flow experiments were carried out using an SF-61 stopped-flow spectrofluorimeter/spectrophotometer from Hi-Tech Scientific (Salisbury, England). The solution in the observation chamber was excited with a 100 W short-arc mercury lamp (Osram, Germany), and the fluorescence was detected at right angles to the incident light beam with an R928 multialkali side-on photomultiplier. The exciting light was passed through a grating monochromator with a blaze wavelength of 500 nm. For experiments using fluorescein-labeled $tRNA^{Phe}$, the mercury line at 436 nm was used for excitation, and the fluorescence was collected at wavelengths ≥475 nm by using an OG475 glass cutoff filter (Schott, Mainz, Germany) in front of the photomultiplier. The kinetic data were collected via a high-speed 12-bit analog-to-digital data acquisition board and were analyzed using software developed by Hi-Tech Scientific. Each kinetic trace consisted of 1024 points. To improve the signal-to-noise ratio, 5−20 experimental traces were averaged before the reciprocal relaxation time was evaluated.

For measurement of absorbance changes, the photomultiplier was adjusted to collect the light passing directly through the mixing chamber. The zero transmission level was set by closing the shutter in front of the photomultiplier.

To measure fast kinetics of Mg^{2+}-induced tRNA folding, one of the drive syringes was filled with the fluorescently labeled tRNA in 20 mM HEPES−KOH, pH 7.8, and the other with the same buffer containing 0.2 or 20 mM $MgCl_2$. After equal volumes of the two solutions were mixed, the final concentration of $MgCl_2$ in the observation chamber was either 0.1 or 10 mM, respectively.

Chemical and Enzymatic Probing. All probing experiments were done using 3′-labeled yeast $tRNA^{Phe}$ in standard buffer containing 20 mM HEPES−KOH, pH 7.8; for native and semidenaturing conditions probing was carried out at 20 °C. 3′-Terminal labeling was performed as described elsewhere (*24*). After labeling, tRNA was purified by high-resolution preparative gel electrophoresis. All enzymes were purchased from Boehringer Mannheim; diethyl pyrocarbonate (DEPC) was purchased from Sigma.

[1] Abbreviations: FITC, fluorescein isothiocyanate; HQS, Mg^{2+}-sensitive fluorescent indicator 8-hydroxyquinoline-5-sulfonic acid.

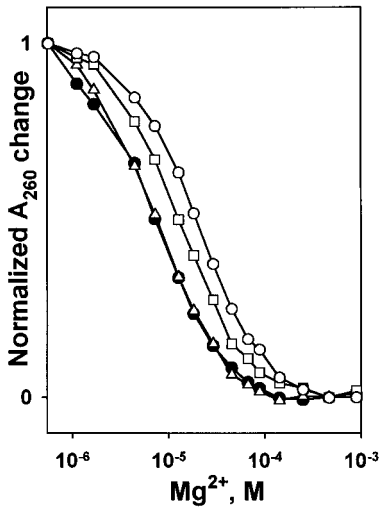

FIGURE 1: Mg^{2+}-induced A_{260} changes of $tRNA^{Phe}$ (filled circles), 3′-Fl $tRNA^{Phe}$ (triangles), D-Fl $tRNA^{Phe}$ (squares), and Y-Fl $tRNA^{Phe}$ (open circles). The plots are not cooperative; the best fit to the Hill equation (eq 1, see text) was obtained when the parameter of cooperativity *n* was set to 1. The beginning of the curves showed substantial deviation from the fit, which probably suggests the presence of an extra low-amplitude transition at <5 μM Mg^{2+}.

DEPC modification and subsequent treatment with aniline as well as enzymatic cleavage reactions were carried out essentially as described (*25*) except that for incubation with DEPC or enzymes the standard buffer (see above) was used. For probing with RNases T1 or V1, tRNA was incubated with 0.2 or 0.3 unit of the corresponding RNase for 10 min.

RNase T1 and acidic ladders were generated as described (*24*). Before application to the gel, all samples were subjected to Cerenkov counting, and equal amounts of radioactive material were applied to each lane.

RESULTS

Mg^{2+}-Induced Conformational Transitions. To monitor conformational changes of yeast $tRNA^{Phe}$, we used tRNA preparations containing fluorescein in one of the following positions: 3′-end (3′-Fl tRNA), anticodon loop, position 37 (Y-Fl tRNA), or D-loop, positions 16 and 17 (D-Fl tRNA). None of these positions are directly involved in tertiary interactions, as seen from the crystal structure of yeast $tRNA^{Phe}$ (*26*). Fluorescent derivatives of $tRNA^{Phe}$ with labels introduced at 16/17 or 37 locations exhibited almost normal aminoacylation efficiency (*27*).

Native mature $tRNA^{Phe}$ was compared with its three fluorescent derivatives by A_{260} measurements at increasing Mg^{2+} concentrations (Figure 1). These experiments were carried out in order to show the preservation of strong Mg^{2+}-binding sites after the modification. The curves for native tRNA and 3′-Fl tRNA virtually coincide, showing the maintenance of all strong Mg^{2+}-binding sites. The curves for D-Fl tRNA and Y-Fl tRNA differ from that for native $tRNA^{Phe}$. This result was anticipated because, according to X-ray data for $tRNA^{Phe}$ crystals, two Mg^{2+}-binding sites are located in the D-loop and anticodon loop (*28*). However, the difference between the dissociation constants for $tRNA^{Phe}$ and 3′-Fl tRNA ($pK_{diss} = 5.14$ for both tRNAs) on one hand and for D-Fl tRNA and Y-Fl tRNA ($pK_{diss} = 4.90$ and 4.74, respectively) on the other is rather small. Changes in ΔG of the transitions caused by the presence of covalently attached

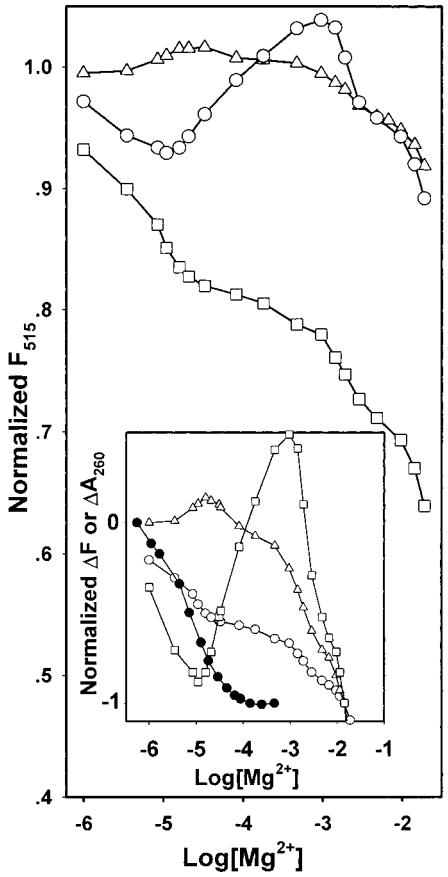

FIGURE 2: Mg^{2+}-induced changes of fluorescence emission of 3′-Fl $tRNA^{Phe}$ (triangles), D-Fl $tRNA^{Phe}$ (squares), and Y-Fl $tRNA^{Phe}$ (circles). Emission was monitored at 515 nm with excitation at 495 nm. The inset shows the same curves and the corresponding Mg^{2+} titration A_{260} curve for unlabeled $tRNA^{Phe}$ (filled circles) normalized by the amplitude of the changes and plotted versus the logarithm of the Mg^{2+} concentration. It shows that the two last fluorescence transitions were not accompanied by A_{260} changes.

labels can be easily estimated from the obtained p*K* values for the unlabeled $tRNA^{Phe}$ and its fluorescent derivatives. Since the plots are not cooperative (see legend to Figure 1), the ΔG change is $2.3RT\Delta pK$. For the worst case of Y-Fl tRNA, the energetic cost associated with the p*K* shift is 0.5 kcal/mol, which is believed to be minor. This implies that, after modification, tRNA conformation remained mostly unaltered. It should be noted that preservation of the binding constants represents a highly sensitive indicator of maintenance of the native structure. For instance, unmodified tRNA transcripts showed about 10-fold weaker Mg^{2+} binding constants as compared to the mature tRNA species (*19*).

We observed strong quenching of fluorescence for all fluorescent tRNA derivatives as compared with free fluorescein in solution and a shift in the maximum of fluorescence toward shorter wavelengths (515 nm instead of 520 nm). This observation probably implies that at all three sites the fluorescent labels strongly interact with surrounding regions of tRNA. Mg^{2+} concentration dependence of the yield of fluorescence for the three fluorescent tRNA derivatives is shown in Figure 2. For all derivatives, four transitions were observed. The amplitudes and directions of the transitions depended on the location of the label. However, the middle points of all four transitions for all three tRNA derivatives virtually coincide. We attribute the observed

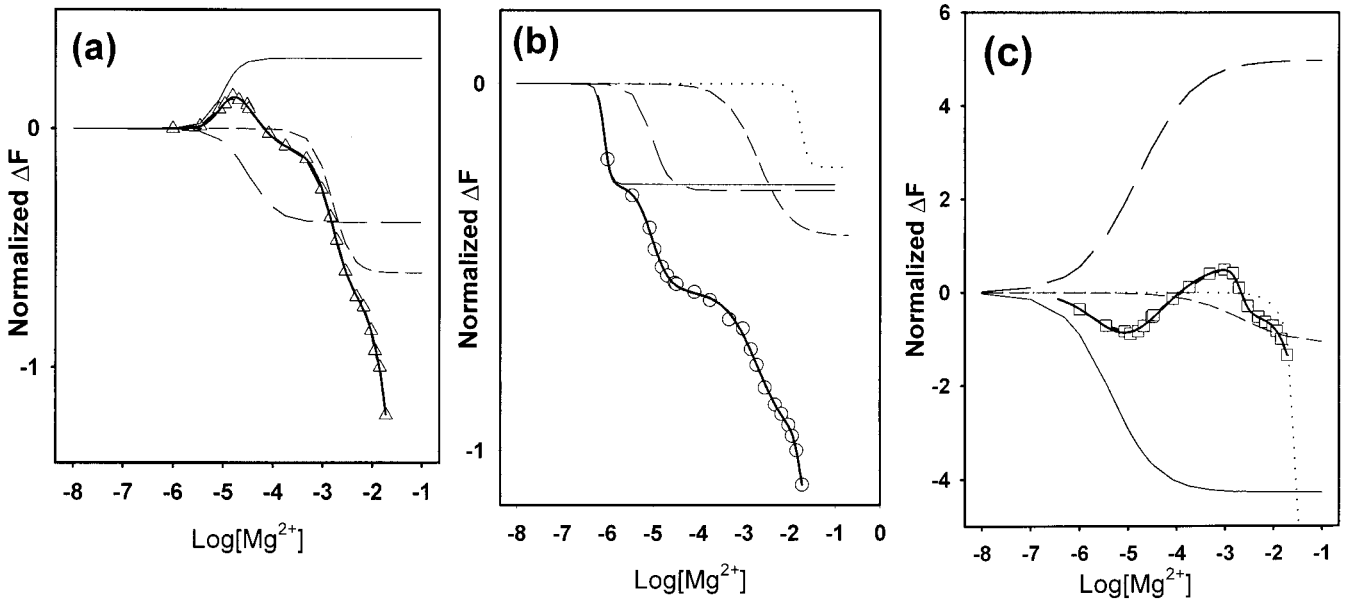

FIGURE 3: Decomposition of the experimental fluorescence titration curves shown in Figure 2 into individual sigmoidal transitions for 3′-Fl $tRNA^{Phe}$ (a), D-Fl $tRNA^{Phe}$ (b), and Y-Fl $tRNA^{Phe}$ (c). For each fluorescent tRNA species, experimental points are shown with the same symbols as in Figure 2. The individual transitions are shown by solid (transition I), long dashed (transition II), short dashed (transition III), and dotted lines (transition IV). The thick lines show the sum of the sigmoids and represent least-squares fits of the experimental titration curves to eq 2. Each sigmoid was plotted according to eq 1 using obtained fit parameters. For all three fluorescent $tRNA^{Phe}$ derivatives a good coincidence between experimental and calculated curves was observed. The parameters of cooperativity were in most cases determined with high experimental error and therefore are not discussed.

changes of fluorescence intensity to conformational transitions of the tRNA molecule resulting from Mg^{2+} binding to distinct types of Mg^{2+}-binding sites. Since the transitions are well separated from each other, it was possible to decompose the experimental curves shown in Figure 2 into individual sigmoidal sections for all three derivatives. Each elementary transition following Mg^{2+} binding to tRNA and causing a change in fluorescence emission intensity ΔI_F may be described by the semiempirical Hill equation:

$$\Delta I_F = A([Mg^{2+}]^n/K^n)/(1 + [Mg^{2+}]^n/K^n) \qquad (1)$$

where K is the Mg^{2+} dissociation constant, A is the total amplitude of emission change, and n is a cooperativity parameter related to the number of bound Mg^{2+} ions required to yield the transition. If four independent transitions take place, then

$$\Delta I_F = \Delta I_{F(1)} + \Delta I_{F(2)} + \Delta I_{F(3)} + \Delta I_{F(4)} \qquad (2)$$

Although in the case of D-Fl tRNA transition I may appear questionable, the use of fewer sigmoid curves (e.g., three instead of four) to fit the data proved to give an unsatisfactory result. Figure 3 shows the decomposition for each of the fluorescent tRNA species. The calculated midpoint Mg^{2+} concentrations for the relevant transitions of the three fluorescent tRNA derivatives appeared to be similar. For the four transitions, the pK_{diss} values averaged from the three titration curves were 5.4, 4.8, 2.7, and 1.7. The inset in Figure 2 shows normalized changes of the fluorescent emission and absorption caused by titration with Mg^{2+}. As seen from these results, the last two transitions with midpoint Mg^{2+} concentrations of 2 and 20 mM were not associated with changes of A_{260}. This implies that these two transitions are not accompanied by alterations in the number of nucleotide pairs.

As mentioned above, the first two fluorescence transitions were apparently accompanied by A_{260} changes. However, as follows from the inset in Figure 2, only one A_{260} transition was observed for unlabeled tRNA, with the apparent K_{diss} value intermediate between those for transitions I and II. The shape of the A_{260} titration curve was not exactly sigmoid; its slope at low Mg^{2+} concentrations indicated that probably an additional transition occurred which could not be distinctly resolved due to its small amplitude. Accordingly, both fluorescence transitions I and II exhibit their absorbance transition counterparts, although the former, with a K_{diss} of a few micromoles, is associated with a relatively small A_{260} change.

Fast Kinetic Steps of tRNA Folding. The stopped-flow technique was used to follow the rapid kinetics of folding caused by a jump in Mg^{2+} concentration. Figure 4 shows the kinetics of absorbance and fluorescence emission changes caused by a Mg^{2+} concentration jump to 0.1 mM. This minimal concentration change should be sufficient to provide Mg^{2+} binding to the strong binding sites of tRNA and convert it from its semidenatured state into its native tertiary structure and D-arm. The kinetics of fluorescence emission appeared to be biexponential, and all three fluorescent derivatives of $tRNA^{Phe}$ showed very similar reciprocal relaxation times. Although the A_{260} curves were usually not smooth, there was a clear accordance between the kinetics of absorbance and fluorescence intensity changes. The biexponential character of the fluorescence kinetics was indicative of two elementary steps of folding, apparently caused by sequential binding of Mg^{2+} to tRNA. The reciprocal relaxation times of the two phases were 1.9 and 28 ms. Further elevation of the Mg^{2+} concentration to 10 mM (a concentration saturating the weak binding sites) had virtually no influence on the kinetics of the A_{260} changes but caused the appearance of an additional slower phase in the fluorescence kinetics (Figure 4c). This behavior agrees with the above steady-state experiments that

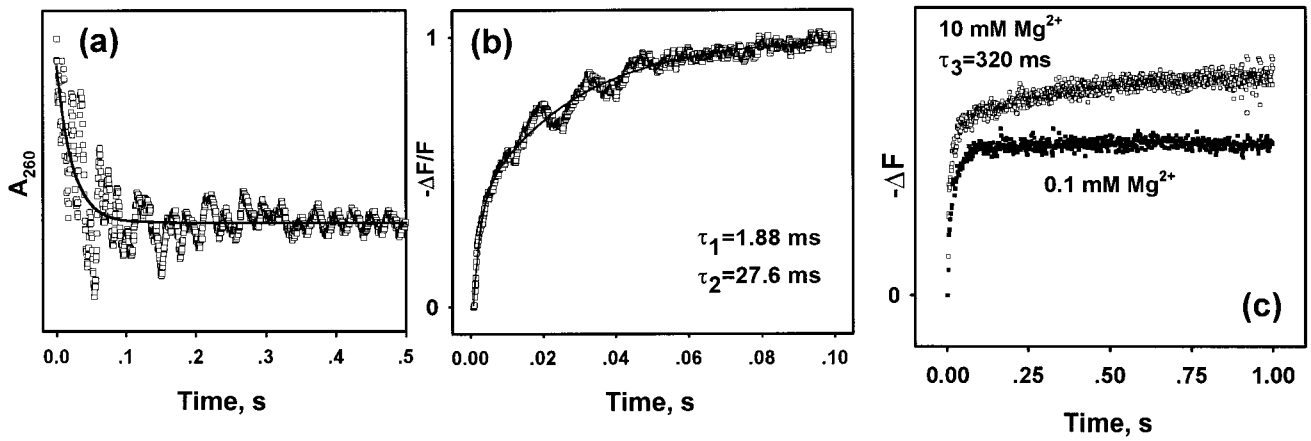

FIGURE 4: (a) Stopped-flow kinetics of A_{260} changes upon Mg^{2+} concentration jump. Mg^{2+} concentration after mixing was 0.1 mM. The solid line represents the fit to a single-exponential time function. (b) Changes of the emission of fluorescence for D-Fl $tRNA^{Phe}$ caused by a jump of the Mg^{2+} concentration to 0.1 mM. The solid line represents a biexponential fit. The calculated reciprocal relaxation times were 1.9 and 28 ms. Two other fluorescent $tRNA^{Phe}$ derivatives exhibited similar reciprocal relaxation times, but the amplitudes of changes were smaller (not shown). (c) Additional slower exponential change yielded by increasing Mg^{2+} concentration to 10 mM (after mixing) as monitored by the emission of 3′-Fl $tRNA^{Phe}$.

showed no extra A_{260} transition at high Mg^{2+} concentrations but demonstrated two fluorescence transitions with midpoints at 2 and 20 mM Mg^{2+}. Therefore, the third phase is likely to correspond to transition III seen in the steady-state Mg^{2+} titration of fluorescent tRNA derivatives. The reciprocal relaxation time of this phase was 320 ms. Thus, in contrast to temperature-jump kinetics where a single Mg^{2+}-dependent transition was found (*29*), the kinetics of fluorescence showed three steps of folding after Mg^{2+} addition, one of them being observed at a high Mg^{2+} concentration only.

As previously shown by the temperature-jump technique, folding of the tRNA tertiary structure and D-stem was rather rapid with a single reciprocal relaxation time of about 7 ms in the absence of Mg^{2+} and 2 ms in the presence of 3 mM Mg^{2+} (*29*). The above experiments also gave 1.9 ms as the fast transition reciprocal relaxation time, but we observed an additional slower phase of fluorescence changes that was not seen in T-jump experiments. Our results on the A_{260} kinetics also suggested the presence of a slower phase (Figure 4a). Therefore, the discrepancy between previous data and our own probably originates from different ionic conditions. For *Escherichia coli* $tRNA^{fMet}$ at high ionic strength (0.17 M Na^+), a single-exponential kinetic transition was coupled with a single stage of tertiary structure and D-arm formation (*29*). The presence of an additional slower component for yeast $tRNA^{Phe}$ suggests a two-step character of formation of the native tertiary structure and D-stem at low concentrations of monovalent ions.

Slow Kinetic Phase after Mg^{2+} Addition. Earlier, slow biexponential renaturation kinetics after Mg^{2+} addition was studied in detail for *E. coli* $tRNA^{Ile}$ (*17*). Yeast $tRNA^{Phe}$ also showed slow kinetics for Mg^{2+}-induced refolding as followed from changes of A_{260} and fluorescence of the attached fluorescent labels over an interval of hundreds of seconds (Figure 5a). The slow-phase kinetics was also biexponential, with reciprocal relaxation times of 20 and 170 s. As was suggested for *E. coli* $tRNA^{Ile}$ and is most probably applicable for yeast $tRNA^{Phe}$, two sequential conformational transitions take place. Since the biexponential origin of slow renaturation was previously analyzed in detail for $tRNA^{Ile}$ (*17*), we focused on the other aspect of this process. We followed

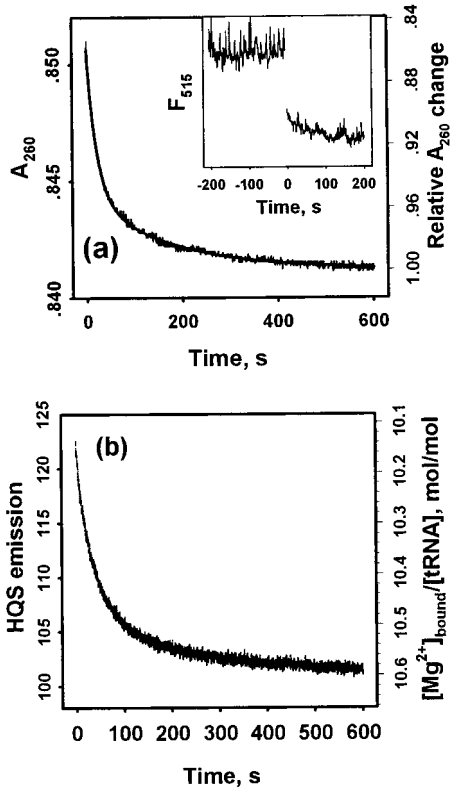

FIGURE 5: (a) Slow renaturation of $tRNA^{Phe}$ caused by addition of Mg^{2+} to 0.05 mM concentration as monitored by A_{260} changes. The solid line represents a biexponential least-squares fit. The calculated reciprocal relaxation times were 23 ± 3 and 170 ± 20 s. The right axis represents the total steady-state amplitude of the A_{260} changes to show the partial amplitude of the slow-phase kinetics. The inset shows the corresponding kinetics of fluorescence emission changes of D-Fl $tRNA^{Phe}$ measured under the same conditions. (b) Kinetics of emission changes of the Mg^{2+}-sensitive fluorescent indicator (HQS; see Materials and Methods) measured as indicated in (a). The $tRNA^{Phe}$ concentration was 2.2 μM. The emission of HQS was proportional to the concentration of free Mg^{2+}. The right axis shows the calculated number of bound Mg^{2+} ions per tRNA molecule. The dashed line represents a biexponential least-squares fit. The calculated reciprocal relaxation times were 21 ± 2 and 180 ± 12 s.

the Mg^{2+} binding in renaturation experiments using a Mg^{2+}-sensitive fluorescent indicator (HQS; see Materials and

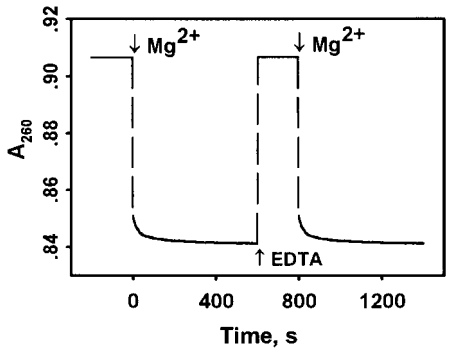

FIGURE 6: Folding and unfolding kinetics of yeast $tRNA^{Phe}$ induced by addition and removal of Mg^{2+}, respectively. The first round of folding was carried out as in Figure 5a, and then EDTA was added to 2 mM to bind Mg^{2+}. The next folding step was initiated by addition of Mg^{2+} to 2.1 mM concentration.

Methods). A weak complex formation between the indicator and Mg^{2+} virtually did not affect their concentrations, and the fluorescence of the indicator was proportional to concentration of free Mg^{2+} (*18*). Figure 5b shows changes of the indicator fluorescence accompanying slow renaturation of tRNA. The right axis refers to the calculated number of bound Mg^{2+} ions during renaturation. The rate constants calculated for the A_{260} (Figure 5a) and Mg^{2+} binding kinetics (Figure 5b) perfectly coincide. It is seen from these data that slow kinetics of tRNA renaturation was accompanied by Mg^{2+} binding. Considering that Mg^{2+} binding itself is a fast process, one can assume that slow conformational rearrangements lead to the formation of new Mg^{2+}-binding sites and by this way limit the observed rate of Mg^{2+} binding.

To learn the origin of the slow kinetic phase in more detail, we examined its reversibility using fast Mg^{2+} removal by an excess of chelating agent (EDTA). Figure 6 shows A_{260} changes of tRNA following EDTA addition after the completion of the first round of Mg^{2+}-induced slow kinetics. As can be seen, after the addition of EDTA the equilibrium was reached in less than a few seconds (time required for mixing) and A_{260} returned to its initial value. Thus, the slow unfolding phase was not observable. Further addition of an excess of Mg^{2+} caused the next round of the slow folding phase. Since fast release of Mg^{2+} in the presence of EDTA took place, Mg^{2+} dissociation/binding should be fast processes. Therefore, the observed slow rate of Mg^{2+} binding (Figure 5b) is limited by slow conformational rearrangements of the tRNA. Furthermore, one can assume that Mg^{2+} bound at the preceding fast kinetic phase (about 10 Mg^{2+} ions/tRNA molecule, Figure 5b) slows down further conformational rearrangements, presumably by stabilization of folding intermediates. The latter assumption is consistent with the strong temperature dependence of the kinetic rate constants. The activation energies, calculated for the faster and slower exponents, were 6.4 and 8.4 kcal/mol, respectively. These values are sufficient for disruption of several base pairs; even larger activation energies have been reported for *E. coli* $tRNA^{Ile}$ (*17*).

It can be seen from the combined data for fast (Figure 4, panels a and c) and slow (Figure 5, panels a and b) kinetics of Mg^{2+}-induced tRNA folding that under these conditions (20 mM HEPES−KOH, 0.1 or 0.05 mM $MgCl_2$, 20 °C) two phases of folding take place that differ in their rates by at least 1000-fold. The fast phase was completed in less than 0.1 s, while the slow phase took longer than 100 s. The amplitudes of the fast changes were much higher than those at the slow phase. A_{260} changes of the slow phase comprised only about 15% of the total amplitude (Figure 5a). During the fast phase, about 10 mol of Mg^{2+} bound/mol of tRNA, while during the slow phase the value was less than 0.5 mol of Mg^{2+} (Figure 5b).

The slow kinetics of Mg^{2+} binding is most probably associated with occupation of newly formed strong Mg^{2+} binding sites. At 0.05 mM about 10 Mg^{2+} ions are bound per tRNA molecule, while solution studies under similar conditions showed the presence of 5 ± 1 strong Mg^{2+} binding sites in yeast $tRNA^{Phe}$ (*18*). Therefore, under the given conditions the strong sites should be saturated. Furthermore, the amplitude of the slow A_{260} kinetics reached a plateau at less than 0.05 mM Mg^{2+} (data not shown), which suggests saturation of the strong Mg^{2+} binding sites. Further increase of Mg^{2+} concentration to saturate the weak binding sites does not affect the amplitude of the kinetics.

Since less than 0.5 mol of Mg^{2+} was bound per mole of tRNA under conditions when all strong sites were saturated, it indicates that only a minor fraction of tRNA molecules accounts for the slow kinetic phase. We assume that an alternative tRNA conformation exists in Mg^{2+}-free solution, which slowly converts after Mg^{2+} addition to the native folded form. It follows from the fast A_{260} relaxation after Mg^{2+} removal that, in the absence of Mg^{2+}, fast exchange between the conformations takes place; otherwise, slow relaxation kinetics of unfolding should be revealed.

Accordingly, after Mg^{2+} addition, the major conformation folding proceeds fast, accounting for the major A_{260} change of the fast kinetic phase (about 85% of the total A_{260} amplitude), while the slow kinetic phase is attributed to folding of the minor conformation.

For both fast and slow relaxations, intermolecular RNA−RNA interactions such as dimerization or aggregation appear not to contribute. In all experiments dealing with fluorescently labeled tRNA, the physical concentration of the sample was low, which should prevent intermolecular interactions. Moreover, no dependence of the kinetic parameters on tRNA concentration was observed.

Chemical and Enzymatic Probing. Chemical and enzymatic probes are widely applied for monitoring conformational changes of RNA (*30*, *31*) and provide information supplementary to that obtained by spectroscopic measurements. We used chemical modifications of adenines with diethyl pyrocarbonate and specific cleavage by RNases T1 and V1 to show changes of base pairing and conformational rearrangements caused by different concentrations of Mg^{2+}. Although the reactivity of different nucleotides in yeast $tRNA^{Phe}$ toward chemical probes (*32*) and nucleases T1 (*33*) and V1 (*34*) was examined in detail, it was important to obtain structural information directly related to the given experimental conditions. Figure 7 shows DEPC modification patterns of 3′-labeled yeast $tRNA^{Phe}$ in denaturing (70 °C), semidenaturing (20 °C, EDTA), and native conditions. As seen, the presence of 0.05 mM Mg^{2+} (lane 6) efficiently protects A14 and A44 from the DEPC modification, indicating the formation of tertiary interactions. Similar protection of these adenines was also observed in the presence of 0.2 M NaCl (lane 7) and 0.02 M NaCl + 10 mM Mg^{2+} (lane 8). Paired adenines located in the helical segments were not

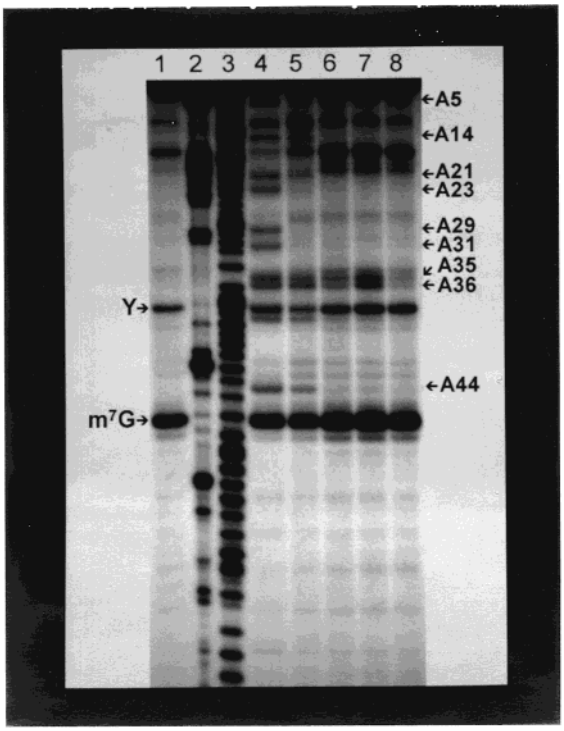

FIGURE 7: Gel electrophoresis of products after DEPC modification of 3′-labeled yeast $tRNA^{Phe}$: lane 1, control incubation without DEPC; lane 2, RNase T1 ladder; lane 3, H^+ ladder. The following lanes show DEPC modification in standard buffer containing the following components: lane 4, standard buffer, 70 °C; lane 5, +1 mM EDTA, 20 °C; lane 6, +0.05 mM $MgCl_2$, 20 °C; lane 7, +0.2 M NaCl + 1 mM EDTA, 20 °C; lane 8, 0.2 M NaCl + 10 mM $MgCl_2$, 20 °C. The standard buffer contained 20 mM HEPES−KOH, pH 7.8.

affected by Mg^{2+} or NaCl and were completely protected when secondary structure was preserved (lanes 5−8). A35 and A36 located in the anticodon were partly protected by 0.05 mM Mg^{2+} but remained reactive in 0.2 M NaCl. A higher concentration of Mg^{2+} (lane 8) was required to ensure their effective protection. These data were consistent with previous findings (*32*) and suggested that formation of tertiary structure is coupled with occupation of the strong binding sites.

Cleavage of yeast $tRNA^{Phe}$ by RNase T1 at different Mg^{2+} concentrations showed (Figure 8a) that Mg^{2+} efficiently protected guanosines, as anticipated from previous studies (*33*). An exception was G20, which showed substantially enhanced cleavage in ≥0.05 mM Mg^{2+}. Since G20 is known to form a Mg^{2+} pocket in yeast $tRNA^{Phe}$ (*1*, *28*), the enhanced susceptibility toward RNase T1 seems to be associated with a local change of G20 conformation due to coordination of the Mg^{2+} ion. For all other G's (including G65 which is not shown), the presence of 0.05 mM Mg^{2+} provided protection against T1 cleavage. However, for all G's the cleavage was enhanced if the Mg^{2+} concentration was increased further. Figure 8b shows the densitometry profile for G30 recorded across lanes 4−10 (Figure 8a). This profile was typical and could represent other G's as well. As can be seen, a transition with a midpoint at 2 mM Mg^{2+} was revealed. Further increase of the Mg^{2+} level from 5 to 20 mM yielded virtually no changes in the cleavage efficiency.

Probing experiments performed with RNase V1 showed that under the given conditions tRNA cleavage was stimulated in the presence of more than 1 mM Mg^{2+} (Figure 9). The positions of the stimulated cleavage are indicated on the right. As can be seen, the millimolar transition was also manifested. RNase V1 is conformation-specific and forms three to four contacts with the phosphates of double-stranded RNA and can also cleave single-stranded regions that are in a stacked helical conformation (*35*). Therefore, on the basis of the stimulation of RNase V1 cleavages, the transition at 2 mM Mg^{2+} seems to bring double-stranded segments of tRNA into the highly stacked helical conformation.

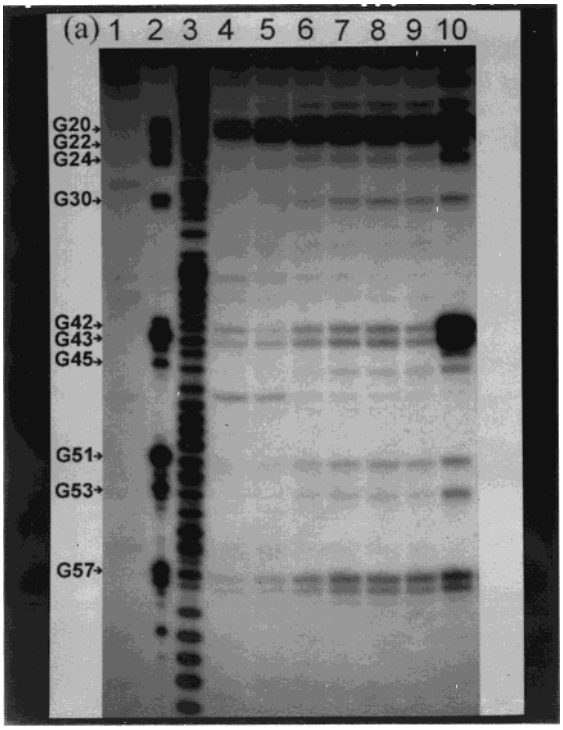

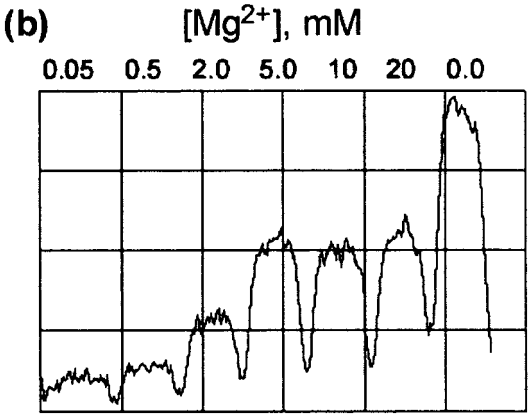

FIGURE 8: (a) Susceptibility of yeast $tRNA^{Phe}$ to cleavage by RNase T1 at different Mg^{2+} concentrations: lane 1, control incubation without RNase T1; lane 2, RNase T1 ladder; lane 3, H^+ ladder. The following lanes correspond to incubation in standard buffer containing the following concentrations of $MgCl_2$: lane 4, 0.05 mM; lane 5, 0.5 mM; lane 6, 2 mM; lane 7, 5 mM; lane 8, 10 mM; lane 9, 20 mM. Lane 10: standard buffer + 1 mM EDTA. For lanes 1 and 4−10, incubation was at 20 °C. (b) A cross-lane densitometry profile of the gel from panel a for the G30 position (lanes 4−10).

We also attempted to examine the structural changes occurring during the slow kinetic phase of tRNA folding using RNase probing. These experiments were performed by increasing the enzyme concentration about 10-fold. After

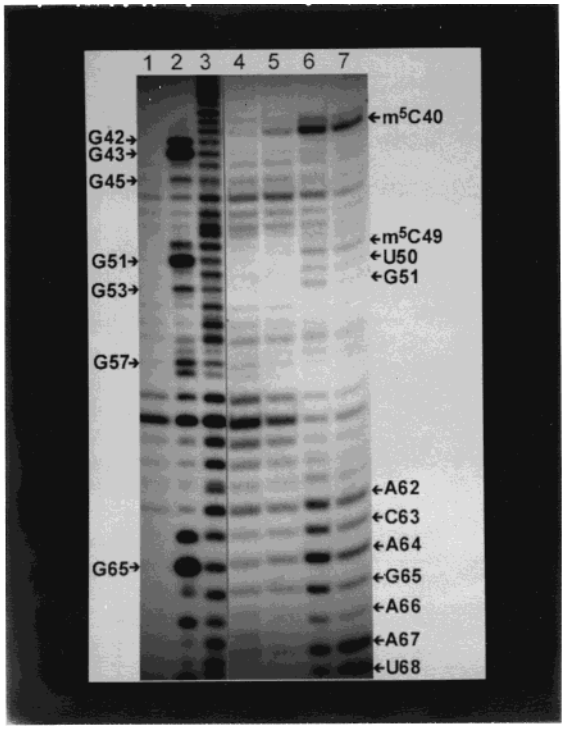

FIGURE 9: Mg^{2+} dependence of RNase V1 cleavages of yeast $tRNA^{Phe}$: lane 1, control incubation in which RNase V1 was omitted; lane 2, RNase T1 ladder; lane 3, H^+ ladder. Lanes 4−7 represent cleavage patterns obtained at the indicated Mg^{2+} concentrations at 20 °C: lane 4, 0.05 mM; lane 5, 1 mM; lane 6, 4 mM; lane 7, 12 mM.

a 1 min incubation the reactions were immediately stopped by phenol extraction. However, no significant differences were observed between digestion patterns obtained with tRNA preincubated with Mg^{2+} and those obtained when Mg^{2+} was added at zero time (data not shown). Apparently, the misfolded structure was represented by a minor fraction of tRNA molecules and therefore could not be revealed in probing experiments.

DISCUSSION

Mg^{2+} Binding and Structural Transitions of tRNA. Mg ions represent an integral part of native RNA structure, and therefore RNA folding is tightly associated with Mg^{2+} binding. Monitoring the conformational changes of RNA caused by Mg^{2+} binding is helpful for understanding the elementary steps of the folding process. To study Mg^{2+}-induced folding of yeast $tRNA^{Phe}$, we have used fluorescent labels covalently attached to three remote positions in the tRNA molecule. In Mg^{2+} titration experiments four conformational transitions were resolved as monitored by fluorescence emission of the labels (Figure 3). The results on the transitions are summarized in Table 1.

Remarkably, the midpoint Mg^{2+} concentrations of the transitions coincide well for all three positions of the labels, although they are located distantly from each other. On the contrary, the sign and amplitude of the emission changes of an individual transition depend on the location of the label. Apparently, the observed conformational changes affect the structure as a whole rather than its local regions and thus cause the concerted, but distinct, response of the labels in remote locations. Since these transitions are caused by Mg^{2+} binding, each of them has to be assigned to distinct types of binding sites that differ in their affinity toward Mg^{2+}. Thus, our data suggest that under the given conditions four types of Mg^{2+} binding exist for $tRNA^{Phe}$. These types can further be subdivided into two classes by their affinity to Mg^{2+}. The first two types, I and II, with K_{diss} of 4 and 16 μM, respectively, are strong Mg^{2+}-binding sites, while the two other types, III and IV, with K_{diss} 2 and 20 mM, respectively, correspond to loose Mg^{2+} binding.

In early studies on Mg^{2+} binding to tRNA a model of two types of noninteracting Mg^{2+}-binding sites ("strong" and "weak", differing in their stability constants by 2−3 orders of magnitude) was applied to account for the roughly biphasic character of the corresponding Scatchard plots (*36*). This model was the simplest to adequately describe the experimental data. Until now the terms strong and weak for Mg^{2+}-binding sites have been widely used in the conventional manner. The data presented in this paper point to the possibility of a more detailed and precise interpretation of the previously obtained Scatchard plots. In particular, on the basis of the above results for Mg^{2+} titration, a model of three types of noninteracting binding sites may be proposed to describe the biphasic Scatchard plots. It follows from decomposition of the fluorescence titration curves (Figure 3) that ~0.5 mM Mg^{2+} concentration initiates transition III. Assuming that transition III represents weak electrostatic binding of Mg^{2+} ions to numerous phosphates of the tRNA backbone (see below), it can substantially contribute to the overall Mg^{2+}-binding stoichiometry and account for the slope of the Scatchard plots in the region of weak binding. Transitions I and II, with K_{diss} of 4 and 16 μM, have to be assigned to two types of strong sites. This model implicates three types of sites, two of which are strong and the third, represented by numerous unspecific sites, is weak. Simulation of Scatchard plots derived from this model using binding parameters found for transitions I−III has shown that the biphasic character of the plots is preserved (not shown) due to the close binding constants for types I and II (Table 1). Many contradictions between Scatchard plots for different conditions mentioned in the literature (*29*, *36*, *37*) might be related to the application of a simplified model to fit the experimental data. For example, at intermediate ionic strength Scatchard plots for Mg^{2+} binding to *E. coli* (*19*) and yeast (Serebrov, unpublished) $tRNA^{Phe}$ are not simply biphasic but are of a more complex nature. After a fast initial slope indicative of the presence of a single strong Mg^{2+}-binding site, they have a distinct bulge that cannot be explained in the framework of the model for two types of binding sites. Alternatively, this bulged region can readily be ascribed to an intermediate class of cooperative sites with a stability constant decreasing at high concentrations of monovalent ions. It is assumed from the results presented here that at low ionic strength such sites are strong, with a stability constant close to that for the unique site found at high monovalent salt concentration.

Some previous findings support the above assumption. While at low ionic strength four to six strong metal ion binding sites are usually found, at high concentration of monovalent ions this number was reduced to only one strong site for different tRNAs (*18*, *19*, *29*, *37*). Thus, one of the strong sites found at low ionic strength is weakly sensitive to competition with an excess of monovalent ions. This

Table 1: Conformational Transitions of Yeast $tRNA^{Phe}$

transition	K_{diss}, M[a]	A_{260}	DEPC	T1	V1	comments
I	$(4 \pm 5) \times 10^{-6}$	±[b]	+[c]	+[c]	+[c]	minor A_{260} changes; strong Mg^{2+} binding to a single specific site
II	$(1.6 \pm 3.2) \times 10^{-5}$	+	+	+	+	strong Mg^{2+} binding; formation of the tertiary structure and D-stem base pairs
III	$(2.0 \pm 1.3) \times 10^{-3}$	−	−	+	+	weak Mg^{2+} binding; no changes in base pairing
IV	$(2.0 \pm 1.0) \times 10^{-2}$	−	−	−	−	

[a] The K_{diss} values were calculated from the decomposition of the fluorescence titration curves (Figure 3). [b] Poorly resolved due to a small amplitude. [c] Transitions I and II were not resolved separately.

implies that in this site the Mg^{2+} ion is specifically coordinated and cannot be easily replaced by a monovalent ion, while the other strong sites correspond to purely electrostatic binding to negatively charged pockets which are much less sensitive to the nature of the positively charged cation. The different modes of Mg^{2+} binding may argue for two types of strong binding sites with different, though close at low ionic strength, stability constants. The existence of specific (or selective) and unspecific strong binding sites has recently been revealed for various RNAs (*38*−*42*).

It should be mentioned that the results on tRNA structural transitions reported in this paper give only indirect clues to the types of Mg^{2+} interactions with tRNA, and the above discussion is aimed only at interpretation of these results in the light of the available data on Mg^{2+} binding to tRNA. Recent studies point to the key role of Coulombic interactions in the Mg^{2+} binding to RNA (*43*, *44*). The theoretical model of purely electrostatic interactions between Mg^{2+} and tRNA based on computation of the total electrostatic potential of the yeast $tRNA^{Phe}$ molecule from its known X-ray structure has very recently demonstrated a good agreement between calculated and experimental parameters of Mg^{2+} binding against the background of monovalent cations (*45*). This model suggests that strong sites are "pockets" possessing negative charges of high density where magnesium ions are retained solely by Coulombic interactions. Interestingly, a similar correlation was also demonstrated by a model assuming electrostatic interactions between Mg^{2+} and a fixed number of *identical* tRNA sites with adjustable binding constants (*37*). The adequacy of the electrostatic model to the experimental data implies that electrostatic interactions are the main driving force for Mg^{2+} binding and RNA stabilization, and contribution of specific interactions, like short-range coordination and hydrogen bonding, may appear questionable. However, some data suggest that at least in some cases a purely electrostatic model fails to explain the experimentally observed Mg^{2+}-binding parameters. In this model with tRNA considered to be a rigid polyelectrolyte molecule, Mg^{2+} binding is always anticooperative. The positive cooperativity of Mg^{2+} binding observed in a certain range of ionic strength (*19*, *37*) is consistent with an interpretation assuming that conformational changes induced by initial Mg^{2+} binding facilitate further binding by increasing the compactness and charge density of the tRNA molecule. At low ionic strength, the Mg^{2+}-binding parameters seem to entirely follow the electrostatic model. However, at high ionic strength, when the electrostatic sites should be occupied by monovalent cations, the initial slope of the Scatchard plot for Mg^{2+} binding strongly deviates from that predicted from the electrostatic model (see, e.g., ref *37*), indicating the presence of a unique specific binding site. This deviation suggests that, at this site, Mg^{2+} is specifically coordinated and cannot be readily substituted by a monovalent cation. Evidently being a location with high-density negative charge, this site must be predicted by the electrostatic model as one of the electrostatic sites.

When this work was accomplished, new results presenting a 2 Å resolution X-ray structure of yeast $tRNA^{Phe}$ emerged (*46*) that provided novel insights into the fine structure of strong Mg^{2+}-binding sites and could serve as a structural basis of the above proposal on existence of a unique strong binding site in this tRNA capable of discrimination between Mg^{2+} and monovalent ions. These results show clearly that one of the detected strong binding sites differs strikingly from the others both in the geometry of the surrounding RNA groups and in the Mg^{2+} coordination type. This site is located in the D-loop and is formed by the phosphate groups of G20 and A21 (site 2). The phosphates of these nucleotides are extremely closely spaced due to a very sharp turn of the tRNA backbone. The Mg^{2+} ion is directly coordinated to the both phosphates, thereby stabilizing the turn. Strikingly, this site is not a typical pocket in the tRNA structure with a cation embedded into it, and its high-density negative charge results from the close proximity of the two phosphate groups. The hydration shell water molecules are not involved in Mg^{2+} coordination, while at other sites they are responsible for a rigid multipoint cation fixation inside the binding pocket. At this site, Mg ion has tetrahedral rather than octahedral configuration. The first distinctive feature of this site is the key one in understanding the origin of its possible selectivity for Mg^{2+} and probably for other multivalent cations as well. The efficient charge neutralization of the two phosphate groups required to maintain their close spacing (the P−P distance = 3 Å) demands a direct Mg^{2+} coordination, with the phosphate oxygen atoms being the ligands involved into the inner coordination sphere of the Mg^{2+}. In this case the octahedral configuration of the coordination sphere becomes disadvantageous because it would undergo a strong distortion resulting from repulsion of the charged phosphate groups. With larger angles between the bonds (109° instead of 90°) and shorter Mg−O distances, the tetrahedral configuration appears to be preferable, as it provides a smaller radius of the coordination sphere together with minimized ligand repulsion. This coordination type is accompanied by a partial Mg^{2+} dehydration that is energy consumable. However, according to theoretical assessments, it proves to be still advantageous if the cation radius is small and the binding site has a high density of negative charge (*42*). The above clarifies the probable mechanism of selectivity toward Mg^{2+} exhibited by the tRNA in the presence of a high concentration of monovalent ions. The structural organization of site 2 and the mode of Mg^{2+} coordination suggest that this site has a strong preference for cations having both a small radius and a high charge and allowing the tetrahedral geometry of the

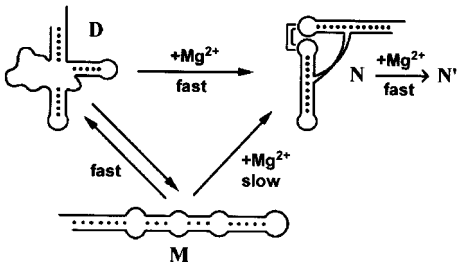

FIGURE 10: Generalized scheme for multiple steps of Mg^{2+}-induced tRNA folding. See text for details.

ligands. It is obvious that monovalent ions, like Na^+ or K^+, do not meet these requirements.

Transition III corresponding to 2 mM Mg^{2+} can be attributed to weak electrostatic Mg^{2+} binding to tRNA backbone phosphates. For short hairpins similar to tRNA arms, Mg^{2+} and other multivalent ions possess small preference for binding to phosphates in both single- and double-stranded regions and exhibit K_{diss} values similar to the value estimated for transition III (*39*, *47*). Effects observed for transition III in probing experiments (Figures 8 and 9) suggest that transition III brings tRNA stems into a more stacked helical state. Therefore, transition III can be associated with considerable conformational changes and could be important for tRNA functions.

Transition IV, with an estimated K_{diss} of 20 mM, probably is not related to tRNA structure in vivo, because such concentrations are far beyond the intracellular Mg^{2+} level. For this transition, the mode of Mg^{2+} binding as well as the origin of the conformational changes is not clear, but its extremely high dissociation constant implies weak diffuse binding resulting in further screening of the tRNA negative charge.

Parallel Pathways of tRNA Folding. The results presented here can be summarized in a generalized scheme shown in Figure 10. On the basis of our data and previous findings we suppose that in the absence of Mg^{2+} and at low concentration of monovalent ions (semidenatured conditions) tRNA partitions between two exchanging conformations, one of which (D) is a cloverleaf tRNA lacking D-stem pairing and tertiary contacts, while the other (M) is an alternative, probably misfolded, species. As follows from known tRNA phase diagrams, the M state can be attributed to the "extended" form found at low ionic strength for several tRNAs (*48*). According to the above data, the M state is only represented by a small fraction of molecules under the given experimental conditions. On the scheme this conformation is shown as an extended bulged hairpin (Figure 10). This structure has been proposed for the low-salt form and suggests an alternative base pairing in the regions of D- and T-arms of tRNA (*48*). Although this model remains speculative, it is supported by recent findings. For example, the human mitochondrial $tRNA^{Lys}$ transcript does not fold into a cloverleaf structure but into an extended bulged hairpin (*49*, *50*). A similar structure has been found for the inactive conformer of *E. coli* $tRNA^{Glu}$ (*51*). Finally, the long bulged hairpin is a near-optimal structure generated for tRNA by algorithms for predicting RNA secondary structures [*mfold* software (*52*)].

In Mg^{2+}-free solution the activation barrier for the exchange between native and misfolded conformations seems to be low. This follows from the fast relaxation of the system after removal of Mg^{2+} by EDTA (Figure 6). After Mg^{2+} addition, both conformations fold into the nativelike structure N (Figure 10). The latter is supposed to be the L-shaped form of tRNA, in which both D-stem and tertiary structure are preserved. It has been demonstrated using the temperature-jump technique that, for the D state, folding is associated with a low activation energy and exhibits fast single-exponential kinetics (*53*). Therefore, the D state can be regarded as a ready-to-fold conformation. However, for the D state at a low ionic strength our data suggest two steps of folding rather than one at high salt concentration.

The slow kinetic phase results from conformer M refolding, which requires a substantial activation energy. Apparently, the Mg^{2+}-stabilized conformation M results in a kinetic trap for the conversion into the native state. It is obvious that this process should be accompanied by partial melting of the misfolded structure M. Therefore, its stabilization increases the activation barrier. These conclusions on the origin of the slow phase are entirely consistent with those made for salt-induced tRNA refolding (*48*). However, the difference in Mg^{2+} and monovalent ion action should be mentioned. While a single elementary transition has been revealed for salt-jump refolding, Mg^{2+} jump results in two folding steps (Figure 5). As pointed out above, in folded tRNA there is a unique specific binding site in which Mg^{2+} cannot be substituted by a monovalent ion, and melting of the tertiary structure leads to release of Mg^{2+} ions from this site (*54*). Thus, monovalent salt alone probably cannot accomplish the conversion, and this explains the difference in kinetics of salt- and Mg^{2+}-induced tRNA refolding.

The observation that at least two conformations of tRNA coexist in solution and their folding pathways are different provides evidence for parallel and simultaneous tRNA folding pathways. It should be pointed, however, that our data do not allow us to judge whether each of the parallel pathways (D to N and M to N) necessarily occurs by strictly sequential steps, although at least for the M to N conversion, sequential steps can be anticipated from previous studies (*17*).

The structure proposed for the misfolded tRNA conformation M and the fact that there is a fast exchange between the native and misfolded conformations suggest that at low salt concentrations not only is the D-stem unpaired but the T-stem is also melted or "breathing". Indeed, the D-to-M conversion (Figure 10) cannot occur without disrupting both the D- and T-stems of the cloverleaf tRNA. Therefore, the fast exchange between D and M implies that under the given conditions the T-stem is destabilized. Accordingly, the low salt region on the equilibrium phase diagram (*48*) might be associated with destabilization or melting of both D- and T-stems.

Evidently, stability of the structure M as well as the rate of its stabilization during Mg^{2+} binding is to be strongly dependent on the tRNA sequence. The primary structure of some tRNAs may rule out any alternative base pairing. For other tRNAs, the Mg^{2+}-dependent alternative folding may be stable enough to make the rate of the M−N transition hardly noticeable. Indeed, the M−D transition induced by an elevated salt concentration (*48*) is characterized by an activation energy varying strongly as dependent on amino acid specificity of tRNA. Therefore, the tRNA stable inactive conformers undergoing transformation into native tRNAs only at an elevated temperature in the presence of Mg^{2+} may

be regarded as the extreme case of misfolding that is typical of many tRNAs. There have been reported stable misfolded structures of *E. coli* tRNAs specific for Glu, Gln, His, and Trp as well as those of yeast $tRNA^{Arg}$ and $tRNA^{Leu}$ (*55*). As mentioned, the stable inactive conformer *E. coli* $tRNA^{Glu}$ has been shown to be a long bulged hairpin (*51*). Similar studies of other tRNAs mentioned above would be of interest for the critical assessment of the above scheme of tRNA folding.

Although the formation of structural elements is accomplished upon Mg^{2+} binding to strong binding sites, our results suggest that further weak binding induces substantial conformational changes of tRNA. The latter could be functionally important. For example, the aminoacylation optimum of yeast $tRNA^{Phe}$ corresponds to 3 mM Mg^{2+} (*27*); this is close to the concentration at which transition III is completed. Therefore, the formation of the N′ structure (Figure 10) at millimolar Mg^{2+} concentrations corresponds presumably to "fine-tuning" of the tRNA molecule that ensures highly specific and efficient recognition and catalysis in the course of protein biosynthesis.

ACKNOWLEDGMENT

We thank E. Gupalo for help in preparation of the manuscript. We are grateful to Dr. M. Zuker for the opportunity to use the on-line version of *mfold* software.

REFERENCES

1. Teeter, M. M., Quigley, G. J., and Rich, A. (1980) in *Nucleic Acid−Metal Interactions* (Spiro, T., Ed.) pp 145−177, Wiley-Interscience, New York.
2. Pan, T., Long, D. M., and Uhlenbeck, O. C. (1993) in *The RNA World* (Gesteland, R., and Atkins, J., Eds.) pp 271−302, Cold Spring Harbor Laboratories, Cold Spring Harbor, NY.
3. Kim, S.-H. (1978) in *Transfer RNA* (Altman, S., Ed.) pp 248−293, MIT Press, Cambridge, MA, and London.
4. Rich, A., Quigley, G., and Teeter, M. (1979) in *Transfer RNA: structure, properties and recognition* (Schimmel, P., Söll, D., and Abelson, J., Eds.) pp 101−113, Cold Spring Harbor Laboratories, Cold Spring Harbor, NY.
5. Pyle, A. M. (1993) *Science 261*, 709−714.
6. Smith, D., and Pace, N. (1993) *Biochemistry 32*, 5273−5281.
7. Zarrinkar, P. P., and Williamson, J. R. (1994) *Science 265*, 918−924.
8. Bassi, G. S., Murchie, A. I. H., Walter, F., Clegg, R. M., and Lilley, D. M. J. (1997) *EMBO J. 16*, 7481−7489.
9. Sclavi, B., Sullivan, M., Chance, M., Brenovitz, M., and Woodson, S. (1998) *Science 279*, 1940−1943.
10. Pan, J., Thirumalai, D., and Woodson, S. A. (1997) *J. Mol. Biol. 273*, 7−13.
11. Treiber, D. K., Rook, M. S., Zarrinkar, P. P., and Williamson, J. R. (1998) *Science 279*, 1943−1946.
12. Draper, D. E. (1996) *Trends Biochem. Sci. 21*, 145−149.
13. Hinz, H.-J., Filimonov, V. V., and Privalov, P. L. (1977) *Eur. J. Biochem. 72*, 79−86.
14. Privalov, P. L., and Filimonov, V. V. (1978) *J. Mol. Biol. 122*, 447−464.
15. Ptitsyn, O. B., Pain, R. H., Semisotnov, G. V., Zerovnik, E., and Razgulyaev, O. I. (1990) *FEBS Lett. 262*, 20−24.
16. Ptitsyn, O. B. (1995) *Trends Biochem. Sci. 20*, 376−379.
17. Lynch, D. C., and Schimmel, P. R. (1974) *Biochemistry 13*, 1841−1852.
18. Römer, R., and Hach, R. (1975) *Eur. J. Biochem. 55*, 271−284.
19. Serebrov, V. Yu., Vassilenko, K. S., Kholod, N. S., Gross, H. J., and Kisselev, L. L. (1998) *Nucleic Acids Res. 26*, 2723−2728.
20. Wimmer, E., Maxwell, I. H., and Tener, G. M. (1968) *Biochemistry 7*, 2623−2628.
21. Hansske, F., and Camer, F. (1979) *Methods Enzymol. 59*, 172−181.
22. Reines, S. A., and Cantor, C. R. (1974) *Nucleic Acids Res. 1*, 767−786.
23. Wintermeyer, W., Schleich, H.-G., and Zachau, H. G. (1979) *Methods Enzymol. 59*, 110−121.
24. Beier, H., and Gross, H. J. (1991) in *Essential Molecular Biology—A Practical Approach* (Brown, T. A., Ed.) Vol. 2, pp 221−236, IRL Press, Oxford, New York, and Tokyo.
25. Krol, A., and Carbon, P. (1989) *Methods Enzymol. 180*, 212−227.
26. Holbrook, S., Sussman, J., Warrant, R., and Kim, S.-H. (1978) *J. Mol. Biol. 123*, 631−660.
27. Wintermeyer, W., and Zachau, H. G. (1979) *Eur. J. Biochem. 98*, 465−475.
28. Holbrook, S. R., Sussman, J. L., Warrant, R. W., Church, G. M., and Kim, S.-H. (1977) *Nucleic Acids Res. 4*, 2811−2820.
29. Stein, A., and Crothers, D. M. (1976) *Biochemistry 15*, 157−160.
30. Ehresmann, C., Baudin, F., Mougel, M., Romby, P., Ebel, J.-P., and Ehresmann, B. (1987) *Nucleic Acids Res. 15*, 9109−9128.
31. Sigman, D. S., and Chen, C. B. (1990) *Annu. Rev. Biochem. 59*, 207−236.
32. Peattie, D. A., and Gilbert, W. (1980) *Proc. Natl. Acad. Sci. U.S.A. 77*, 4679−4682.
33. Wrede, P., Wurst, R., Vournakis, J., and Rich, A. (1979) *J. Biol. Chem. 254*, 9608−9616.
34. Lockard, R. E., and Kumar, A. (1981) *Nucleic Acids Res. 9*, 5125−5140.
35. Lowman, H. B., and Draper, D. E. (1986) *J. Biol. Chem. 261*, 5396−5403.
36. Schimmel, P., and Redfield, A. (1980) *Annu. Rev. Biophys. Bioeng. 9*, 181−221.
37. Leroy, J., and Guéron, M. (1977) *Biopolymers 16*, 2429−2446.
38. Wang, Y.-X., Lu, M., and Draper, D. E. (1993) *Biochemistry 32*, 12279−12282.
39. Laing, L. G., Gluick, T. C., and Draper, D. E. (1994) *J. Mol. Biol. 237*, 577−587.
40. Basu, S., Rambo, R. P., Strauss-Soukup, J., Cate, J. H., Ferré-D'Amaré, A. R., Strobel, S. A., and Doudna, J. A. (1998) *Nat. Struct. Biol. 5*, 986−992.
41. Cate, J. H., Hanna, R. L., and Doudna, J. A. (1997) *Nat. Struct. Biol. 4*, 553−558.
42. Draper, D. E., and Misra, V. K. (1998) *Nat. Struct. Biol. 5*, 927−930.
43. Hermann, T., and Westhof, E. (1998) *Structure 6*, 1303−1314.
44. Chin, K., Sharp, K. A., Honig, B., and Pyle, A. M. (1999) *Nat. Struct. Biol. 6*, 1055−1061.
45. Misra, V. K., and Draper, D. E. (2000) *J. Mol. Biol. 299*, 813−825.
46. Jovine, L., Djordjevic, S., and Rhodes, D. (2000) *J. Mol. Biol. 301*, 401−414.
47. Laing, L. G., and Draper, D. E. (1994) *J. Mol. Biol. 237*, 560−576.
48. Cole, P. E., Yang, S. K., and Crothers, D. M. (1972) *Biochemistry 11*, 4358−4368.
49. Helm, M., Brulé, H., Degoul, F., Cepanec, C., Leroux, J.-P., Giegé, R., and Florentz, C. (1998) *Nucleic Acids Res. 26*, 1636−1643.
50. Helm, M., Giegé, R., and Florentz, C. (1999) *Biochemistry 38*, 13338−13346.
51. Madore, E., Florentz, C., Giegé, R., and Lapointe, J. (1999) *Nucleic Acids Res. 27*, 3583−3588.
52. Walter, A. E., Turner, D. H., Kim, J., Lyttle, M. H., Muller, P., Mathews, D. H., and Zuker, M. (1994) *Proc. Natl. Acad. Sci. U.S.A. 77*, 4079−4082.
53. Cole, P. E., and Crothers, D. M. (1972) *Biochemistry 11*, 4368−4374.
54. Stein, A., and Crothers, D. M. (1976) *Biochemistry 15*, 160−168.
55. Lindahl, T., Adams, A., and Fresco, J. R. (1966) *Biochemistry 55*, 941−948.

BI002241P